12^{th} International Conference on Fracture Mechanics of Concrete and Concrete Structures
FraMCoS-12
B.L.A. Pichler, Ch. Hellmich, P. Preinstorfer (Eds)

https://doi.org/10.21012/FC12.1213
MS02-2:5

MODELING OF TEMPERATURE- AND RATE-DEPENDENT FATIGUE BEHAVIOR OF CONCRETE CAPTURING THE THERMO-VISCOPLASTIC EFFECTS ON MATERIAL DEGRADATION

Rostislav Chudoba[1], **Miroslav Vořechovský**[2] **Mario Aguilar**[1], **Abedulgader Baktheer**[1]

[1] Institute of Structural Concrete, RWTH Aachen University,
Mies-van-der-Rohe-Str. 1 52074 Aachen, Germany, maguilar@imb.rwth-aachen.de

[2] Institute of Structural Mechanics, Brno University of Technology,
Veveří 95, 602 00 Brno, Czech Republic

Key words: Concrete fatigue, Thermodynamics, Damage, Viscoplasticity, Temperature

Abstract. Concrete fatigue testing is costly and time-intensive, often requiring high loading frequencies to reduce durations, which impacts fatigue performance due to heat generation. This highlights the need for a robust model to capture the interaction between loading rate and temperature, aiding experimental interpretation and enabling faster testing—an area that is not yet addressed by current modeling approaches. This contribution aims to introduce a unified, thermodynamically-based constitutive model describing concrete behavior. The model integrates viscoplastic effects with cumulative sliding damage as mechanisms driving the material degradation. Additionally, the effect of temperature is integrated into the thermodynamic framework, coupled with viscoplastic strains, so that the intrinsic heat generation from internal friction is accounted for. Furthermore, Gibbs free energy-based formulation facilitates the stress-driven fatigue simulations at the single material point idealization. Elementary studies examining the behavior of concrete under uniaxial compression are used to analyze the effects of both loading-rate and thermal factors on both monotonic and fatigue behavior.

1 INTRODUCTION

Accurate predictions of the service life of critical concrete infrastructure under fatigue loading are essential, especially given the fast-changing strategies in global energy supply. A major challenge, however, is the limited understanding of concrete fatigue behavior—a key contributor to the early failure of many structures, preventing them from achieving their anticipated service life [1, 2, 3, 4].

Fatigue testing of concrete is a time-intensive and costly process, often requiring several weeks to complete. To address these limitations, high-cycle fatigue behavior is commonly studied using relatively high loading frequencies (5–10 Hz), which substantially shorten the test duration and reduce costs [5, 6]. However, it is well established that loading frequency significantly impacts fatigue behavior, particularly affecting the number of cycles to fatigue failure, as depicted in the Wöhler or S−N curve [7]. Beyond the influence of loading frequency, heat generation within the specimen during cyclic loading has emerged as a critical factor affecting fatigue life. Recent experimental studies have demonstrated that this thermal buildup significantly impacts the fatigue performance of concrete [8, 9, 10, 11]. This effect is particularly pronounced in fatigue tests conducted at high frequencies, where the rapid cyclic loading induces substantial temperature increases within the specimen. An overview

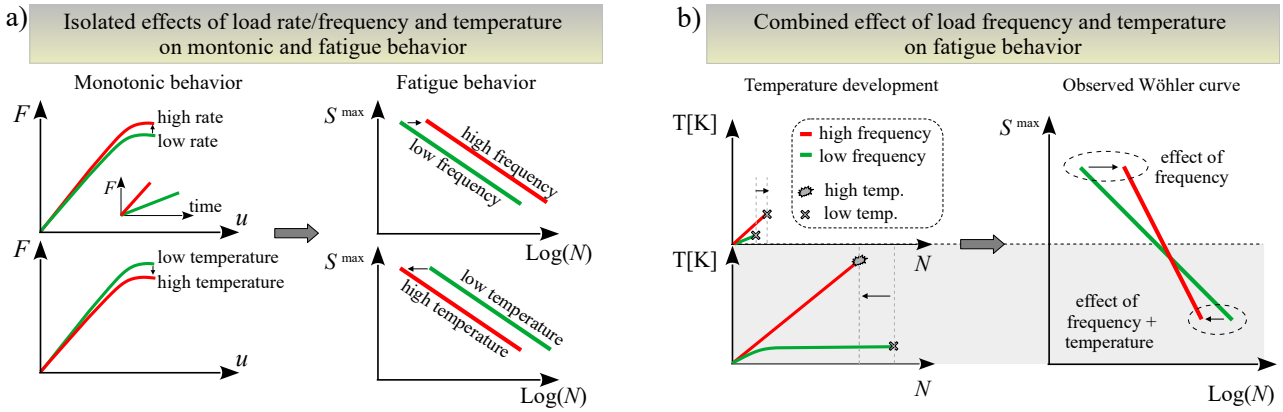

Figure 1: Summary of the interacting effects of rate/frequency and temperature on the concrete monotonic and fatigue behavior; (a) individual effects separately; (b) combined effects

of the observed trend due to the interaction of loading frequency and temperature is shown in Fig. 1.

Over the past few decades, several modeling approaches have been developed to describe the fatigue compressive behavior of concrete. Phenomenological lifetime-based approaches, which use the number of loading cycles as the primary variable governing damage, have been widely proposed [12, 13]. For more detailed cycle-by-cycle simulations, tensorial models have been formulated, where fatigue damage is correlated with strain measures [14, 15, 16]. Recently, more advanced models capable of simulating fatigue stress redistribution within a single material point have been introduced, leveraging frameworks such as the microplane model or lattice discrete modeling approaches [17, 18, 19, 20]. Despite these advancements, the complex interplay between loading rate and temperature and its influence on concrete fatigue behavior remains unaddressed in existing numerical models.

To address this gap, this contribution introduces a thermodynamics-based framework for fatigue modeling that accounts for the effects of loading rate and temperature. In analogy to previously developed cycle-by-cycle models, a single material point idealization is adopted to reproduce the fatigue behavior of concrete observed in cylindrical specimens. To examine material degradation, the framework employs the simplest possible formulation of thermodynamic potentials capable of capturing the experimentally observed trends, providing a foundation for more comprehensive future developments within macro- and meso-scale models.

2 GENERALIZED MATERIAL

The algebraic structure of the thermodynamically based Generalized Standard Material (GSM) model has been implemented using the computer algebra system sympy [21], which automatically generates a time-stepping algorithm based on the specified potentials for free energy and dissipation. To verify and demonstrate the feasibility and functionality of the framework, an example of compression-induced concrete fatigue is implemented for a single material point.

2.1 Helmholtz free energy

The work and heat transfer to and from the material are controlled and monitored through the strain ε, the absolute temperature ϑ, and the reference temperature ϑ_0. The state of the material is represented by viscoplastic strain, isotropic hardening, kinematic hardening, and damage, which are arranged in the vector of internal/state variables $\boldsymbol{\mathcal{E}} = \{\varepsilon_{\mathrm{vp}}, z, \alpha, \omega\}$. The Helmholtz free energy is expressed as the sum of energy contributions from viscoplastic damage, hardening, and thermal effects as

$$\psi(\vartheta, \varepsilon, \boldsymbol{\mathcal{E}}) = \psi_{\mathrm{mech}} + \psi_{\mathrm{therm}}, \qquad (1)$$

where

$$\psi_{\text{mech}} = \frac{1}{2\rho} E\,(1-\omega)\,(\varepsilon - \varepsilon_{\text{vp}})^2 \tag{2}$$

$$+ \frac{1}{2\rho} K z^2 + \frac{1}{2\rho}\gamma\alpha^2, \tag{3}$$

and

$$\psi_{\text{therm}} = c_\varepsilon \left(\vartheta - \vartheta \ln \frac{\vartheta}{\vartheta_0} \right), \tag{4}$$

with c_ε representing the thermal capacity measured at constant strain in the thermo-elastic regime of the material. The conjugate forces are obtained as

$$\boldsymbol{\mathcal{S}} = \frac{\partial \psi}{\partial \boldsymbol{\mathcal{E}}} = \{-\sigma, Z, X, -Y\}^T, \tag{5}$$

where the individual variables represent the total stress σ, hardening forces Z and X, and the stored elastic energy Y. The negative signs ensure that σ and Y remain positive as their conjugate variables—namely the viscoplastic strain ε_{p} and damage ω. The entropy is then conjugate to the temperature via

$$s = -\frac{\partial \psi}{\partial \vartheta} = c_\varepsilon \ln \frac{\vartheta}{\vartheta_0}. \tag{6}$$

2.2 Threshold function and flow rule

To account for the effect of damage on the evolving elastic limit, the apparent stress σ must be modified by relating it to the undamaged (intact) fraction of the material, yielding an effective stress $\frac{\sigma}{1-\omega}$. To demonstrate a minimal setup for simulating concrete fatigue that also includes thermal effects, we define the following threshold function

$$f := \left| \frac{\sigma}{1-\omega} - X - X_0 \right| - (f_{\text{c}} + Z)\, e^{-\beta(\vartheta - \vartheta_0)},$$

where X_0 represents the initial offset of the elastic domain, f_{c} is the compressive strength, ϑ_0 is the initial temperature, and β controls the rate of temperature-induced shrinkage of the elastic domain.

To account for the evolution of damage ω, the flow potential φ follows the Lemaitre concept [22] and includes both the threshold function f and the conjugate variable Y

$$\varphi = f + (1-\omega)\,\frac{S}{1+r}\left(\frac{Y}{S}\right)^{r+1}. \tag{7}$$

Finally, the evolution equations of the rate-independent damage-plasticity are obtained as

$$\dot{\boldsymbol{\mathcal{E}}} = \lambda \frac{\partial \varphi}{\partial \boldsymbol{\mathcal{S}}}, \tag{8}$$

where λ represents the inelastic multiplier. The discrete time-integration algorithm is derived by discretizing the consistency condition

$$\dot{f}\,(\boldsymbol{\mathcal{E}}, \boldsymbol{\mathcal{S}}(\boldsymbol{\mathcal{E}})) = 0, \quad \lambda \geq 0, \quad \lambda \dot{f} = 0. \tag{9}$$

An iterative scheme for obtaining the admissible internal variables and the plastic multiplier follows the approach described in [23].

2.3 Viscoplastic regularization

The rate-dependency is incorporated via the viscoplastic regularization [24]. Given the rate-independent solution for the current time increment Δt, the plastic multiplier $\Delta\lambda_\infty$ obtained from (8) is scaled using the relaxation time τ, which depends on the viscosity, elastic moduli, and hardening moduli. The final plastic multiplier and the relaxation time are

$$\Delta\lambda = \frac{\Delta t/\tau}{1 + \Delta t/\tau}\Delta\lambda_\infty, \; \tau = \frac{\eta}{E + K + \gamma} \tag{10}$$

2.4 Thermo-mechanical coupling

Both reversible and irreversible processes are included in the present combination of the first and second laws of thermodynamics. Thermo-mechanical coupling includes irreverisble according to the derivation scheme presented for example in [25, 26]. The rate of change of internal energy $\dot{u}$ equals the the rate of external work $\sigma\dot{\varepsilon}$ plus the the heat transfer q

$$\rho\dot{u} = \sigma\dot{\varepsilon} + q. \tag{11}$$

In case of adiabatic process considered in the demonstrative examples here, $q = 0$. Using

the relation between the rates of internal energy, Helmholtz free energy, entropy and temperature

$$\dot{u} = \dot{\psi} + s\dot{\vartheta} + \vartheta\dot{s}. \tag{12}$$

The rate of Helmholtz free energy becomes

$$\dot{\psi} = \frac{\partial\psi}{\partial\vartheta}\dot{\vartheta} + \frac{\partial\psi}{\partial\varepsilon}\dot{\varepsilon} + \frac{\partial\psi}{\partial\boldsymbol{\mathcal{E}}}\dot{\boldsymbol{\mathcal{E}}}. \tag{13}$$

The rate of entropy $\dot{s}$ can be obtained using (6)

$$\dot{s} = -\frac{\partial\dot{\psi}}{\partial\vartheta} = -\frac{\partial^2\psi}{\partial\vartheta^2}\dot{\vartheta} - \frac{\partial^2\psi}{\partial\vartheta\partial\varepsilon}\dot{\varepsilon} - \frac{\partial^2\psi}{\partial\vartheta\partial\boldsymbol{\mathcal{E}}}\dot{\boldsymbol{\mathcal{E}}}. \tag{14}$$

Substituting for $\dot{\psi}$ and $\dot{s}$ in (12), and using the relation $s = -\partial\psi/\partial\vartheta$ after rearrangements, we obtain the heat balance equation (11) as

$$\cancel{\frac{\partial\psi}{\partial\vartheta}\dot{\vartheta}} + \cancel{\frac{\partial\psi}{\partial\varepsilon}\dot{\varepsilon}} + \frac{\partial\psi}{\partial\boldsymbol{\mathcal{E}}}\dot{\boldsymbol{\mathcal{E}}} + \cancel{s\dot{\vartheta}} + \vartheta\left(\underbrace{-\frac{\partial^2\psi}{\partial\vartheta^2}}_{c_\varepsilon/\vartheta}\dot{\vartheta} - \frac{\partial^2\psi}{\partial\vartheta\partial\varepsilon}\dot{\varepsilon} - \frac{\partial^2\psi}{\partial\vartheta\partial\boldsymbol{\mathcal{E}}}\dot{\boldsymbol{\mathcal{E}}}\right) = \cancel{\frac{1}{\rho}\sigma\dot{\varepsilon}} \tag{15}$$

Substituting the first-order derivatives with respect to the external variables ε and ϑ by their conjugate variables σ and s, and using the fact that, as derived for instance in [27], the second-order derivative with respect to temperature corresponds to the heat capacity c_ε measured in the elastic regime at constant strain, i.e.

$$s = -\frac{\partial\psi}{\partial\vartheta},\ \sigma = \rho\frac{\partial\psi}{\partial\varepsilon},\ c_\varepsilon = -\vartheta\frac{\partial^2\psi}{\partial\vartheta^2}, \tag{16}$$

the heat balance condition provides the evolution equation for the temperature

$$c_\varepsilon\dot{\vartheta} = \vartheta\frac{\partial^2\psi}{\partial\vartheta\partial\varepsilon}\dot{\varepsilon} + \left(\vartheta\frac{\partial^2\psi}{\partial\vartheta\partial\boldsymbol{\mathcal{E}}} - \frac{\partial\psi}{\partial\boldsymbol{\mathcal{E}}}\right)\dot{\boldsymbol{\mathcal{E}}}. \tag{17}$$

The total amount of dissipation, encompassing all irreversible mechanisms, contributes to the generated temperature. Note that this approach allows for an explicit association between each dissipative mechanism and the resulting temperature increase. For example, plastic dissipation may be the primary source of temperature rise, while other externally observable phenomena such as acoustic emission can be attributed to damage dissipation.

2.5 Gibbs free energy for fatigue loading

In order to enable elementary studies of stress-controlled fatigue load scenarios at the level of a one-dimensional compression model, the implemented GSM framework provides an automatic derivation of the Gibbs free energy $\phi(\sigma, \vartheta; \boldsymbol{\mathcal{E}})$ via the Legendre transformation

$$\phi(\sigma, \vartheta, \boldsymbol{\mathcal{E}}) = \psi(\varepsilon, \vartheta, \boldsymbol{\mathcal{E}}) - \frac{1}{\rho}\sigma\,\varepsilon.$$

By inverting the constitutive relation

$$\sigma = \frac{\partial\psi}{\partial\varepsilon} = \Sigma(\varepsilon) \quad \Longrightarrow \quad \varepsilon = \Sigma^{-1}(\sigma),$$

we obtain the stress-controlled state function

$$\phi(\sigma, \vartheta; \boldsymbol{\mathcal{E}}) = \sigma\,\Sigma^{-1}(\sigma) - \psi\big(\Sigma^{-1}(\sigma), \vartheta; \boldsymbol{\mathcal{E}}\big). \tag{18}$$

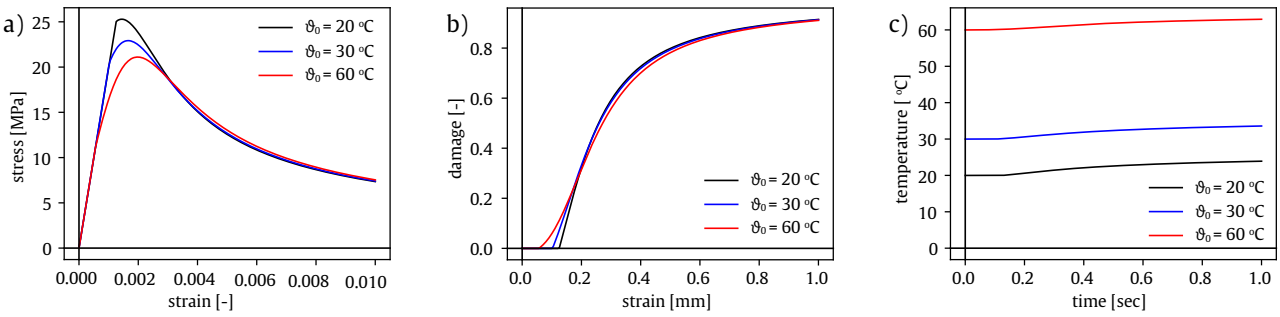

E = 20000 MPa, K = 0 MPa, γ =50000 MPa, f_c = 25 MPa, S = 1.0 x 10^{-5} MPa, c = 2.0, r = 1.0,
c_ε = 1.0 x 10^{-4} J/g-K, β = 0.02, η = 1000 MPa·s

Figure 2: Elementary study on the influence of temperature on the monotonic behavior under compression: a) stress-strain response; b) corresponding damage evolution; c) temperature evolution

The implemented GSM framework accepts the state function in both the form of (12) and (18). The automated derivation scheme for the time-integration procedure, including the backward Euler scheme, return mapping, and viscoplastic regularization (employing the symbolic algebra package sympy [21]), remains the same for both versions of the potential.

3 MONOTONIC COMPRESSION

Following the standard approach in fatigue testing, the first step is to identify the material strength using a monotonic compression test [28]. As is well known from experimental observations, this strength is significantly influenced by both the loading rate and the temperature [11]. In this section, we examine the ability of the model to qualitatively capture this dependence.

3.1 Effect of temperature

The compressive behavior of concrete under varying temperature levels is shown in Fig. 2. Three distinct temperature levels were investigated to highlight the detrimental effect of temperature increase on concrete strength, consistent with findings reported in [29]. This reduction in strength is clearly reflected in the stress-strain responses displayed in Fig. 2a. The corresponding damage evolution is depicted in Fig. 2b. Additionally, Fig. 2c illustrates the temperature evolution during loading, where the increase is linked to energy dissipation during the inelastic deformation process, as detailed in Sec. 2.4. The material parameters used in the model for this study are summarized in Fig. 2.

3.2 Effect of loading rate

To examine the influence of loading rate on the compressive monotonic response, three distinct loading rates were considered, as shown in Fig. 3a. To investigate the relationship between damage evolution and the resulting compressive strength under different loading rates, two scenarios are presented in Fig. 3. In the first scenario (Fig. 3c), damage growth remains relatively slow or negligible up to the point of ultimate strength. The corresponding stress–strain responses in Fig. 3b show a clear trend of increasing strength with higher loading rates, consistent with experimental observations reported by various authors (e.g., [11, 30]). This behavior is attributed to the viscoplastic characteristics of the proposed model.

In contrast, when relatively large levels of damage are permitted to develop up to the ultimate strength—as illustrated in Case 2, Fig. 3e—the rapid damage growth produces a reversed trend: the compressive strength decreases as the loading rate increases (Fig. 3d). This highlights a limitation of the single-degree-of-freedom, single-material-point idealization, which consolidates all dissipative effects into a single variable. At the macroscale, concrete behavior arises from dissipative processes developing in multiple orientations within the material. More advanced approaches, such as microplane or lattice discrete models, can capture this phenomenon more accurately because they account for the anisotropic evolution of damage. Under uniaxial compression, damage in the loading direction is minimal and primarily emerges in perpendicular or tangential directions, as noted in prior studies [17] Consequently, the macroscale compressive behavior is expected to be governed primarily by viscoplasticity, making Case 1 in the first row of Fig. 3 more representative of the true loading-rate effect. This aspect will be explored further in future publications employing microplane and lattice discrete models.

4 FATIGUE LOADING

Even though the specified potentials are minimalistic, they can still be combined with the GSM solver to reproduce the observable thermo-mechanical fatigue behavior of concrete, including the formation of hysteretic loops with gradual increases in damage and total strain. Two illustrative examples are presented, demonstrating the rate- and temperature-dependence of the fatigue response of concrete specimens under compression. In

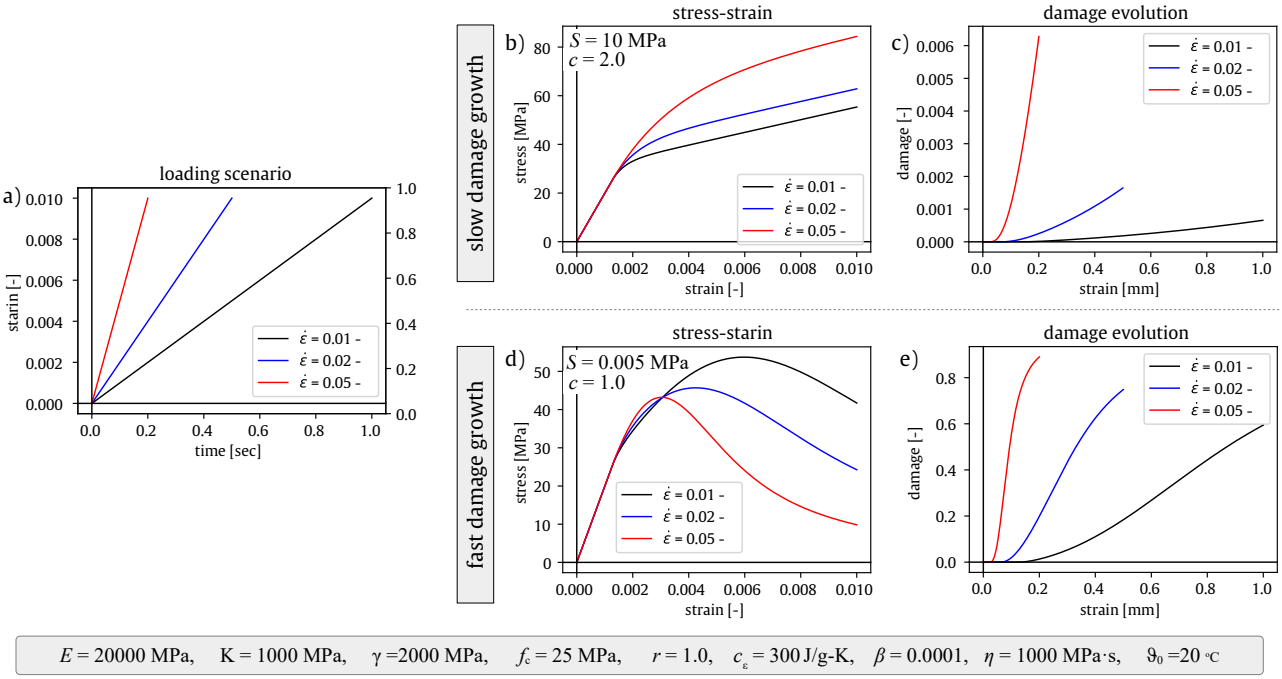

Figure 3: Elementary study of monotonic behavior under varied loading rates: a) loading histories; b, c) stress-strain response and damage evolution (case 1: slow damage growth); d,e) stress-strain response and damage evolution (case 2: rapid damage growth)

both examples, the same set of material parameters is used, specifically: $E = 50$ MPa, $\gamma = 49.5$ MPa, $K = 500$ MPa, $S = 0.08$ MPa, $c = 7.5$, $r = 2.7$, $f_c = 44$ MPa, $\eta = 20000$ MPa s, $\vartheta_0 = 20$, $C_v = 0.0001$ J/kg^{-1} K^{-1}, $\beta = 0.001$. To examine the ability of the model to qualitatively reproduce the thermo-mechanical and viscosity-related trends inherent in fatigue compression tests, the effect of loading frequency on the fatigue degradation process and the number of cycles to failure is investigated for a loading frequency of 1 Hz (Fig. 4) and 50 Hz (Fig. 5). In both studies, uniform stress-controlled uniform cyclic fatigue loading with 10^5 load cycles has been applied using four levels of upper load $S_{\max} \in [0.95, 0.85, 0.75, 0.7]$ and constant lower load $S_{\min} = 0.1$.

4.1 Slow fatigue loading

For the low-frequency loading, the stress–strain diagrams in Fig. 4 demonstrate the model's ability to reproduce the development of hysteretic loops. While fatigue failure occurred for $S_{\max} \in \{0.95, 0.85\}$, lower fatigue loading with $S_{\max} \in \{0.75, 0.70\}$ did not reach failure within 10^5 cycles.

To illuminate the fatigue-driving mechanisms in the irreversible regime, the elastic domain displayed in Fig. 4 illustrates the effect of kinematic hardening, which pulls the elastic domain during the first cycle into the compression regime. It also indicates the inelastic behavior during both loading and unloading, accompanied by the irreversible evolution of internal variables.

In this context, these curves highlight an important aspect of thermodynamics-based fatigue modeling. For example, considering the curve for $S_{\max} = 0.95$, which fails after 23 cycles, we observe that the elastic domain moves downward inelastically during all unloading steps. Without this dissipation during unloading, the subsequent loading steps would remain on the path of the previous loading steps, and fatigue degradation would cease.

Furthermore, let us note that the size of the elastic domain evolves with the increasing number of cycles. Focusing on $S_{\max} = 0.85$ in Fig. 4, we observe an expansion of the elastic regime from the beginning to the middle of

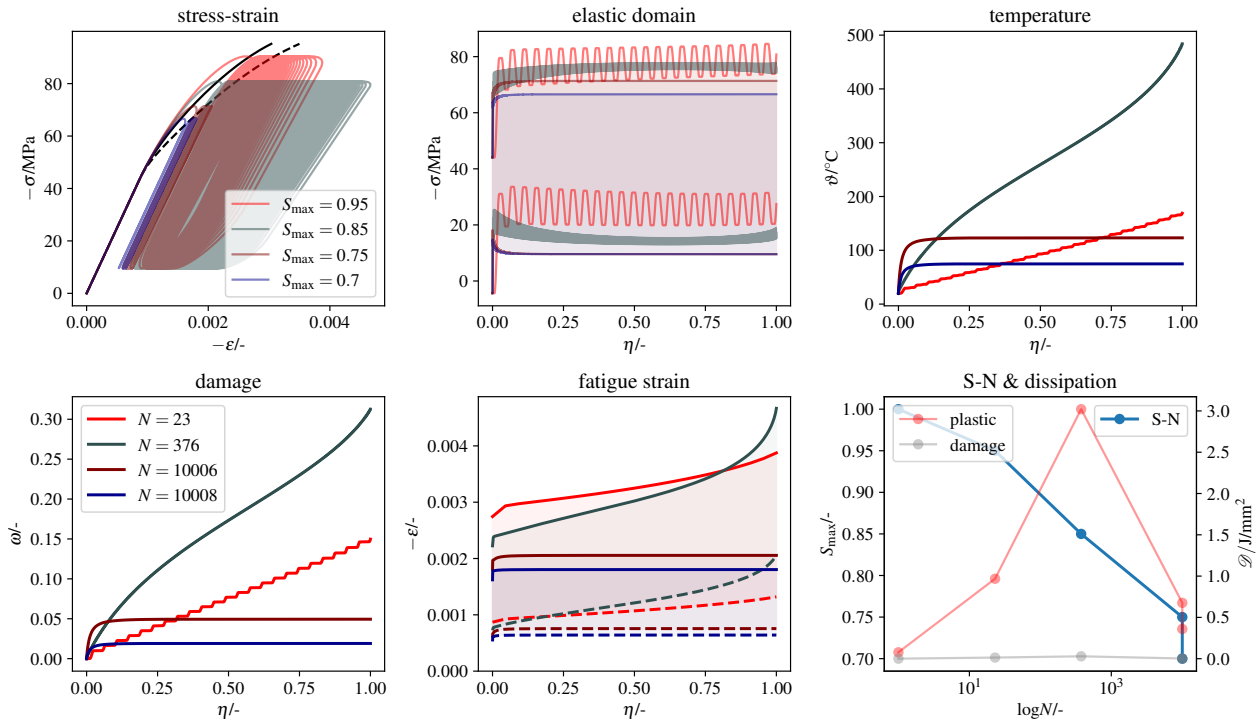

Figure 4: Fatigue response illustrating the interaction between viscosity and intrinsic temperature development under adiabatic conditions at a loading frequency of 1 Hz.

the lifetime, followed by its subsequent shrinkage. This development demonstrates the interplay between isotropic hardening at the onset and the opposing effects of cumulative damage and temperature increase. The temperature obtained for this test after 376 cycles is unrealistically high. This is because the intrinsic heat generated due to thermo-mechanical coupling could not escape, as no heat flux from the material was considered.

The qualitative development of damage, fatigue strain, and the S-N curve displayed in the second row show plausible trends. The fatigue strain in the middle diagram exhibits a rapid increase in strain increments between cycles, which is related to the stronger effect of isotropic hardening during the early stages of fatigue loading. The second branch shows the stable growth of fatigue strain, followed by a rapid increase due to high temperature and cumulative damage once the lifetime exceeds $\eta > 0.75$.

To present the results in a form relevant for fatigue design assessment, the bottom-right diagram shows the S-N curve. Simultaneously, it presents the cumulative energy due to plastic degradation mechanisms and damage. Apparently, plastic dissipation dominated and increased significantly during fatigue loading, while damage-induced dissipation remained small and did not change significantly for the studied loading histories.

Let us remark that the low loading frequency did not activate the viscous effects in the response.

4.2 Rapid fatigue loading

The same load levels were applied in Fig. 5 with a loading frequency of 50 Hz. The high-rate loading activated viscous effects, which increased the inelastic range during each load cycle. As a result, degradation was accelerated, and all four levels of $S_{\max}$ failed within the studied range of 10^5 cycles. The difference in the degradation process is evident from the comparison of the evolution of the elastic domains in Figs. 4 and 5. Specifically, during rapid loading, the elastic domain moves only slowly to-

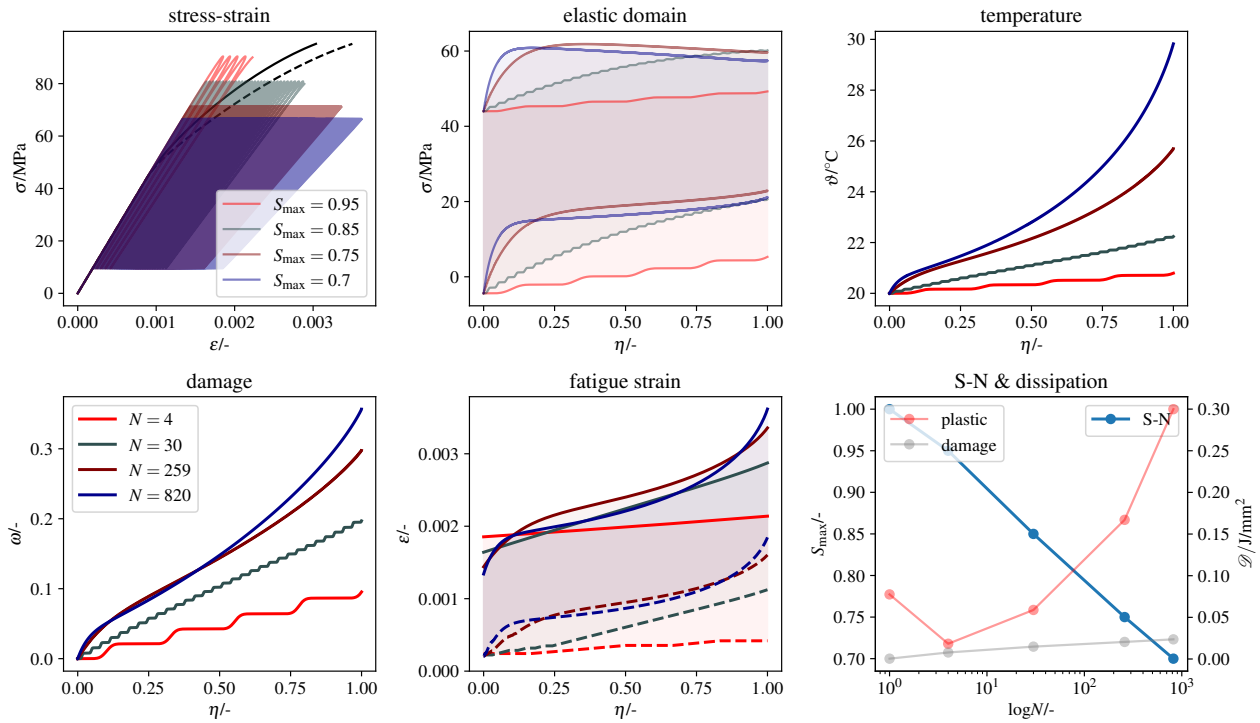

Figure 5: Fatigue response illustrating the interaction between viscosity and intrinsic temperature development under adiabatic conditions at a loading frequency of 50 Hz.

wards overstress, resulting in a larger inelastic range during each cycle and thus a faster degradation process.

It is also interesting to note that for low fatigue loading, $S_{\max} = 0.7$, only a very small inelastic range is active during unloading. Nonetheless, this small inelastic range is sufficient to accumulate the necessary amount of damage, initiating the final branch of fatigue localization as indicated in the bottom-middle diagram of Fig. 5.

Finally, the results summarized in the bottom-right diagram, presented as an S-N curve in a semi-logarithmic scale, confirm a linear trend. The qualitative trends observed for 1 Hz loading in Fig. 4 are similar to those observed for 50 Hz loading. The rates of plastic and damage dissipation are significantly slower due to the lower number of cycles to failure.

5 CONCLUSIONS

In this work, we have proposed a thermodynamically consistent constitutive framework that rigorously captures the interplay of rate- and temperature-dependent mechanisms in concrete fatigue. By deriving the governing equations directly from thermodynamic potentials, we ensure a physically robust treatment of dissipative processes, the evolution of state variables, and damage accumulation. This approach, currently formulated at a single material point, already demonstrates its effectiveness for investigating how internal friction-induced heating, loading rates, and fatigue interact.

The single-point constitutive model presented here is an important and necessary first step toward a full thermo-mechanical description of concrete's fatigue behavior. By firmly establishing the fundamental dissipative and state-variable evolution laws at the material-point level, we lay the groundwork for future expansions.

Looking ahead, the symbolic framework based on the concept of a general standard material offers substantial benefits for developing material models that can be effortlessly integrated into advanced solvers for initial boundary value problems. This framework can be

utilized in a variety of applications, including finite element models that employ microplane models, as well as in fully discrete thermo-mechanical simulations. Such applications can address complex interaction between fatigue degradation, effect of loading rate end temperature.

In this form, the full potential of the thermodynamically based constitutive law will become accessible within general numerical simulators, enabling a more comprehensive and realistic predictions of concrete fatigue. Understanding the influence of loading rate and temperature will also enable the accurate reinterpretation of accelerated fatigue tests and the application of results to real-world scenarios. Similarly, more precise predictions based on in situ data, accompanied by temperature recordings, will enhance the reliability of the model in practical applications.

ACKNOWLEDGEMENT

The work was supported within the framework of the joint project *Energy dissipation-based approach to stochastic fatigue of concrete considering interacting time and temperature effects*, supporting the German partner by the German Research Foundation (DFG), project number 471796896, and the Czech partner (M. Vořechovský) by the Czech Science Foundation, project number GF22-06684K.

REFERENCES

[1] B. Schmidt, S. Schneider, S. Marx, Concrete fatigue-safety and development potential of current design concepts, Bautechnik 96 (4) (2019) 329–337.

[2] A. Baktheer, C. Goralski, J. Hegger, R. Chudoba, Stress configuration-based classification of current research on fatigue of reinforced and prestressed concrete, Structural Concrete (2024). doi:10.1002/suco.202300667.

[3] M. Aguilar, A. Baktheer, H. Becks, M. Classen, R. Chudoba, Fatigue-induced concrete fracture under combined compression and shear studied using standard cylinder and refined punch-through shear test setup, 11th International Conference on Fracture Mechanics of Concrete and Concrete Structures (2023). doi:10.21012/FC11.092350.

[4] M. Aguilar, A. Baktheer, R. Chudoba, On the energy dissipation in confined concrete subjected to shear cyclic loading, Proceedings in Applied Mathematics and Mechanics 22 (1) (2023) e202200301. doi:10.1002/pamm.202200301.

[5] S. Schneider, R. Herrmann, S. Marx, Development of a resonant fatigue testing facility for large-scale beams in bending, International Journal of Fatigue 113 (2018) 171–183. doi:10.1016/j.ijfatigue.2018.03.036.

[6] A. Baktheer, H. Spartali, R. Chudoba, J. Hegger, Concrete splitting and tip-bearing effect in the bond of anchored bars tested under fatigue loading in the push-in mode: An experimental investigation, Materials and Structures 55 (3) (2022) 101. doi:10.1617/s11527-022-01935-7.

[7] S. Schneider, D. Vöcker, S. Marx, Zum Einfluss der Belastungsfrequenz und der Spannungsgeschwindigkeit auf die Ermüdungsfestigkeit von Beton, Beton- und Stahlbetonbau 107 (12) (2012) 836–845. doi:10.1002/best.201200054.

[8] J. Hümme, C. Haar, L. Lohaus, S. Marx, Fatigue behaviour of a normal-strength concrete – number of cycles to failure and strain development, Structural Concrete 17 (4) (2015) 637–645. doi:10.1002/suco.201500139.

[9] N. Oneschkow, J. Hümme, L. Lohaus, Compressive fatigue behaviour of high-strength concrete in a dry and wet environ-

ment, Construction and Building Materials 262 (2020) 119700. doi:10.1016/j.conbuildmat.2020.119700.

[10] M. Deutscher, N. L. Tran, S. Scheerer, Experimental investigations on temperature generation and release of ultra-high performance concrete during fatigue tests, Applied Sciences 10 (17) (2020). doi:10.3390/app10175845.

[11] A. Baktheer, R. Chudoba, Experimental study of the interacting effects of loading rate and temperature on concrete fatigue behavior under compression, Construction and Building Materials 458 (2025) 139466. doi:10.1016/j.conbuildmat.2024.139466.

[12] A. Baktheer, R. Chudoba, Classification and evaluation of phenomenological numerical models for concrete fatigue behavior under compression, Construction and Building Materials 221 (2019) 661 – 677. doi:10.1016/j.conbuildmat.2019.06.022.

[13] D. Pfanner, Zur Degradation von Stahlbetonbauteilen unter Ermüdungsbeanspruchung, Ph.D. thesis, Ruhr-Universität Bochum, Bochum, Germany: (2003).

[14] A. Alliche, Damage model for fatigue loading of concrete, International Journal of Fatigue 26 (9) (2004) 915–921. doi:10.1016/j.ijfatigue.2004.02.006.

[15] R. Desmorat, F. Ragueneau, H. Pham, Continuum damage mechanics for hysteresis and fatigue of quasi-brittle materials and structures, International Journal for Numerical and Analytical Methods in Geomechanics 31 (2) (2007) 307–329. doi:10.1002/nag.532.

[16] A. Baktheer, E. Martínez-Pañeda, F. Aldakheel, Phase field cohesive zone modeling for fatigue crack propagation in quasi-brittle materials, Computer Methods in Applied Mechanics and Engineering (2024) 116834doi:10.1016/j.cma.2024.116834.

[17] A. Baktheer, M. Aguilar, R. Chudoba, Microplane fatigue model MS1 for plain concrete under compression with damage evolution driven by cumulative inelastic shear strain, International Journal of Plasticity 143 (2021). doi:10.1016/j.ijplas.2021.102950.

[18] A. Baktheer, S. Esfandiari, M. Aguilar, H. Becks, M. Classen, R. Chudoba, Fatigue-induced stress redistribution in prestressed concrete beams modeled using the constitutive hypothesis of inter-aggregate degradation, Fatigue & Fracture of Engineering Materials & Structures (2024). doi:10.1111/ffe.14388.

[19] M. Aguilar, A. Baktheer, R. Chudoba, Multi-axial fatigue of high-strength concrete: Model-enabled interpretation of punch-through shear test response, Engineering Fracture Mechanics 311 (2024) 110532. doi:10.1016/j.engfracmech.2024.110532.

[20] M. Aguilar, A. Baktheer, R. Wan-Wendner, J. Vorel, M. Vořechovský, R. Chudoba, Simulation of tri-axial stress redistribution effect in concrete under fatigue loading: Lattice discrete model vs. microplane model, The 9th European Congress on Computational Methods in Applied Sciences and Engineering, ECCOMAS Congress (2024).

[21] A. Meurer, C. P. Smith, M. Paprocki, O. Čertík, S. B. Kirpichev, M. Rocklin, A. Kumar, S. Ivanov, J. K. Moore, S. Singh, T. Rathnayake, S. Vig, B. E. Granger, R. P. Muller, F. Bonazzi, H. Gupta, S. Vats, F. Johansson, F. Pedregosa, M. J. Curry, A. R. Terrel, v. Roučka, A. Saboo, I. Fernando, S. Kulal, R. Cimrman, A. Scopatz, Sympy:

symbolic computing in python, PeerJ Computer Science 3 (2017) e103. doi:10.7717/peerj-cs.103.

[22] J. Lemaitre, A course on damage mechanics, Springer Science & Business Media, 2012. doi:10.1007/978-3-642-18255-6.

[23] R. Chudoba, M. Vořechovský, M. Aguilar, A. Baktheer, Coupled sliding–decohesion–compression model for a consistent description of monotonic and fatigue behavior of material interfaces, Computer Methods in Applied Mechanics and Engineering 398 (2022) 115259. doi:10.1016/j.cma.2022.115259.

[24] J. C. Simo, T. J. Hughes, Computational inelasticity, Vol. 7, Springer Science & Business Media, 2006.

[25] W. Egner, H. Egner, Thermo-mechanical coupling in constitutive modeling of dissipative materials, International Journal of Solids and Structures 91 (2016) 78–88. doi:10.1016/j.ijsolstr.2016.04.024.

[26] A. Berezovski, J. Engelbrecht, G. A. Maugin, Generalized thermomechanics with dual internal variables, Archive of Applied Mechanics 81 (2) (2011) 229–240. doi:10.1007/s00419-010-0412-0.

[27] N. S. Ottosen, M. Ristinmaa, The Mechanics of Constitutive Modeling, Elsevier, 2005.

[28] A. Baktheer, R. Chudoba, Experimental and theoretical evidence for the load sequence effect in the compressive fatigue behavior of concrete, Materials and Structures 54 (2) (2021) 82. doi:10.1617/s11527-021-01667-0.

[29] M. Deutscher, M. Markert, S. Scheerer, Influence of temperature on the compressive strength of high performance and ultra-high performance concretes, Structural Concrete 23 (4) (2022) 2381–2390. doi:10.1002/suco.202100153.

[30] A. I. Abdullah, Effects of loading rates on concrete compressive strength, IOP Conference Series: Materials Science and Engineering 1144 (1) (2021) 012033. doi:10.1088/1757-899X/1144/1/012033.